Results in Optics 21 (2025) 100917

Contents lists available at ScienceDirect

Results in Optics

journal homepage: www.sciencedirect.com/journal/results-in-optics

A symmetric dual-ring cross stub based dual-band THz metamaterial absorber design for permittivity sensing applications

Ahmed Alqurashi [a,*], Sayeeda Khanam [b], Esam Y.O. Zafar [a], Ahmed J.A. Al-Gburi [c,*]

[a] Department of Electrical Engineering, Umm Al Qura University, Makkah 24382, Saudi Arabia
[b] Department of Electrical and Electronic Engineering, International Islamic University Chittagong (IIUC), Kumira, Sitakunda, Chattogram 4318, Bangladesh
[c] Center for Telecommunication Research & Innovation (CeTRI), Fakulti Teknologi Dan Kejuruteraan Elektronik Dan Komputer (FTKEK), Universiti Teknikal Malaysia Melaka (UTeM), Jalan Hang Tuah Jaya, 76100 Durian Tunggal, Melaka, Malaysia

ARTICLE INFO

Keywords:
Terahertz (THz)
Metamaterial
Absorber
High-sensitivity
Permittivity

ABSTRACT

This paper presents a novel dual-band terahertz (THz) metamaterial absorber based on a symmetric dual-ring cross-stub (SDR-CS) resonator, designed for high-sensitivity permittivity sensing. The absorber, composed of aluminum resonators and a polyamide substrate, features a compact unit cell of 80 × 80 μm with rotational symmetry. It exhibits two strong absorption peaks at 1.26 THz and 2.29 THz with near-unity absorption. Detailed electromagnetic simulations reveal the physical mechanisms underpinning the dual-band response and confirm polarization insensitivity and angular stability up to 60° incidence under TE and TM polarizations. Crucially, the device demonstrates excellent sensing performance for refractive indices in the range 1.0–3.162, achieving sensitivities of 0.148 THz/RIU (148 GHz/RIU) and 0.28 THz/RIU (280 GHz/RIU) at the lower and higher resonance frequencies, respectively. The quality factors (Q) are 32.3 and 39.3, resulting in figure-of-merits (FOM) of 39.3 and 32.3 RIU–1, outperforming many reported metamaterial sensors with larger sizes or more complex materials. These attributes underscore the absorber's potential as a compact, efficient, and highly sensitive platform for THz permittivity sensing with applications in biomedical diagnostics, chemical identification, and environmental monitoring.

1. Introduction

Metamaterials (MMs) represent an innovative frontier in electromagnetic wave handling, offering engineered artificial media whose properties are unattainable in natural materials. In particular, the terahertz (THz) frequency range (0.1–10 THz) has attracted growing attention for its potential applications across imaging, sensing, and communication systems (Bisht et al., 2025; Shao et al., 2025). Metamaterial absorbers (MAs) have emerged as crucial devices due to their ability to produce high absorption efficiency within an ultrathin structure, overcoming traditional limitations such as the quarter-wavelength thickness constraint of traditional absorbers (Chen et al., 2022; Nipun et al., 2025; Nipun et al., 2025; Nipun et al., 2025; Hakim et al., 2022). The localized resonance effects within metamaterials allow for strong confinement of electromagnetic fields, which directly enhances interaction with analytes placed in close proximity, making these devices extremely sensitive. Among various advances, dual-band THz absorbers have gained importance because they provide multi-frequency sensing capabilities, enhancing detection accuracy and flexibility in operating frequencies. Designing absorbers that simultaneously achieve dual-band operation with high-quality factors (Q-factors) and optimal sensitivity remains challenging due to trade-offs in geometry, material choices, and fabrication constraints (Pahadsingh and Appasani, 2024). Permittivity/refractive index-based sensing harnesses changes in the dielectric properties of materials, primarily the complex permittivity (ε), as a way to detect and characterize analytes. Since permittivity profoundly influences the refractive index and thus the electromagnetic resonance conditions of metamaterials, its modulation is directly translated into measurable shifts in the resonance frequencies or absorption characteristics (Pahadsingh and Appasani, 2024; Wang et al., 2024). This approach enables label-free, minimally invasive detection with excellent resolution. In practice, small perturbations in permittivity near the metamaterial resonator result in detectable shifts in resonant frequency, which can be utilized for real-time monitoring of analytes presence and concentration.

In 2010, Na Liu et al. introduced a plasmonic sensor based on

* Corresponding authors.
E-mail addresses: akqurashi@uqu.edu.sa (A. Alqurashi), ahmedjamal@ieee.org (A.J.A. Al-Gburi).

https://doi.org/10.1016/j.rio.2025.100917
Received 4 August 2025; Received in revised form 12 October 2025; Accepted 13 October 2025
Available online 14 October 2025

infrared perfect metamaterial absorbers (MAs) (Liu et al., 2010), achieving a figure of merit (FOM) nearly four times greater than that of sensors utilizing plasmonic gold nanorods. This breakthrough sparked widespread interest in applying MAs for sensing purposes, quickly becoming a prominent research focus. Subsequently, numerous MAs have been developed for diverse sensing applications, including micro-electromechanical system (MEMS) sensors (Xu et al., 2022), temperature sensors (Linyang et al., 2021), humidity sensors (Nie et al., 2020), pressure sensors (Hakim et al., 2021), and refractive index sensors (Shruti and Appasani, 2024). As terahertz (THz) technology advanced, the field of terahertz sensing gained prominence, leading to rapid growth in terahertz metamaterial absorbers (TMAs) designed for sensing. Several strategies have been proposed to enhance the sensing performance of TMAs. For example, Longqing Cong et al. demonstrated two TMA designs with experimentally verified higher sensitivity than planar metasurfaces, employing single metal pattern layers on silicon substrates (Cong et al., 2015). Xin Hu et al. developed a TMA-integrated microfluidic sensor that leverages concentrated electromagnetic fields in etched dielectric spacers between metal layers for improved analyte interaction and sensitivity (Hu et al., 2016). Hong Zhou et al. proposed a bilayer cross-shaped plate–hole TMA structure, achieving high sensitivity by spatially overlapping electromagnetic hot-spots with the analyte (Zhou et al., 2019). Building on these foundations, numerous high-sensitivity TMAs for refractive index sensing have since been reported (Chen, 2023). For instance, Nipun et al. (2025) reported a dual-band lantern-shaped TMA on a lead glass substrate exhibiting near-perfect absorption (99.997 % at 9.7 THz and 98.46 % at 10 THz) with high thermal stability, polarization, and incident angle insensitivity, making it suitable for environmental monitoring applications (Nipun et al., 2025). Similarly, their triple-band interconnected oval-shaped split-ring TMA achieved high quality factors and enhanced figures of merit, enabling precise refractive index detection for gas sensing with excellent linearity (Nipun et al., 2025). Several recent works have reported dual-band or high Q-factor THz metamaterial absorbers. For instance, Wang et al. (2023) demonstrated a dual-band absorber at ~0.89 and 1.36 THz with >99 % absorption and notable Q-factors, but restricted to smaller refractive-index ranges (Wang et al., 2023). Shruti et al. (2023) presented a reconfigurable absorber for gas sensing with Q ~87, yet only for refractive index (RI) changes between 1.00 and 1.03 (Shruti et al., 2023). More recently, Sensors (2025) published an all-metal metamaterial absorbers with enhanced sensitivity, though still with limitations in RI range and single or narrow band behavior (Banerjee et al., 2025). Despite these advances, many reported designs still suffer from limitations, such as narrow refractive index sensing ranges (≤2.0), reliance on expensive materials like gold, and relatively large footprints that restrict integration into compact platforms. These shortcomings limit their practicality for real-world applications. To overcome these challenges, this work is motivated by the need for a dual-band THz absorber that combines wider sensing range, enhanced Q-factors and FOM, compact geometry, and fabrication-friendly materials. By using aluminum and polyamide, the proposed design offers a cost-effective, scalable, and high-performance alternative for THz sensing.

To address this gap, this paper proposes a symmetric dual-ring cross-stub (SDR-CS) based THz metamaterial absorber using aluminum and polyamide. The absorber achieves dual-band near-perfect absorption at 1.26 THz and 2.29 THz with polarization insensitivity, angular stability up to 60°, and an extended sensing range of 1.0–3.162. Unlike many previous studies that relied on gold and polyimide, the use of aluminum and polyamide ensures a cost-effective and fabrication-friendly solution while maintaining high sensitivity and figures of merit. These contributions clearly distinguish the proposed design from prior works, as summarized in the comparison presented in Table 1.

Table 1
Peak frequency for different permittivity values of MUT.

Permittivity	Refractive index	Frequency (THz)	Frequency (THz)
1	1.000	1.2622	2.3347
2	1.414	1.2027	2.2684
3	1.732	1.1725	2.1787
4	2.000	1.1569	2.1514
5	2.236	1.114	2.1319
6	2.449	1.0633	1.9759
7	2.645	1.0243	1.9213
8	2.828	0.9853	1.8394
9	3.000	0.9619	1.7887
10	3.162	0.9424	1.7302

2. Metamaterial absorber design

The proposed Symmetric Dual-Ring Cross Stub (SDR-CS) metamaterial absorber is engineered to operate in the terahertz (THz) frequency regime, leveraging subwavelength resonant structures to achieve near-perfect absorption. The unit cell is composed of three primary layers: a patterned aluminum (Al) resonator on the top, a polyimide dielectric substrate, and a continuous aluminum ground plane at the bottom. The absence of transmission through the metallic backing ensures that absorption is solely governed by reflection suppression, where absorption $A(\omega)$ is defined as (Hakim et al., 2022a; Landy et al., 2008; Hakim et al., 2022b):

$$A(\omega) = 1 - \left|S_{11}^2\right| - \left|S_{21}^2\right|$$

$$A(\omega) = 1 - \left|S_{11}^2\right| \quad (1)$$

Considering the transmission coefficient $S_{21}\approx 0$ due to the opaque metal backing. The symmetrical nature of the SDR-CS geometry ensures polarization insensitivity under normal incidence. This design strategy allows for tailoring the resonance characteristics by varying structural parameters such as ring radii, stub length, and substrate thickness, making it suitable for sensing and stealth applications in the THz band. The unit cell design, shown in Fig. 1(a and b), features two concentric circular rings with four radially symmetric stubs (cross arms) connecting the rings. This SDR-CS geometry introduces multiple electric and magnetic dipole moments under electromagnetic excitation, facilitating multiband and/or broadband resonance. The symmetry of the configuration ensures polarization insensitivity under normal incidence, an important feature for practical sensing and stealth applications. The periodicity, outer and inner ring radii *R2* and *R1*, stub width *RW*, and substrate thickness *ht* were optimized through parametric sweeps to tailor the resonance behavior in the target frequency band. The multi-resonator effect from dual rings and stubs enables strong field confinement and enhances absorption efficiency at specific THz frequencies due to impedance matching with free space. The resonator and ground layers are both realized using aluminum (Al), a cost-effective and commonly used conductive material for THz applications due to its high conductivity and ease of deposition. In CST Microwave Studio, the conductivity of aluminum is defined as: $\sigma = 3.56 \times 10^7$ S/m. The substrate material is polyimide, a flexible, low-loss dielectric with favorable mechanical and chemical stability. Its relative permittivity and loss tangent are set as: =3.5, tanδ = 0.0027. These values enable adequate confinement of the electromagnetic field within the substrate while minimizing dielectric losses. The selection of polyimide also makes the absorber compatible with flexible or conformal THz absorber applications.

The dielectric response of the polyimide substrate can be explained using the Debye relaxation theory, which describes the frequency-dependent behavior of complex permittivity. According to the Debye model, the permittivity is expressed by equation (2) (Zhao et al., 2013)

$$\varepsilon(\omega) = \varepsilon_\infty + \frac{\varepsilon_s - \varepsilon_\infty}{1 + j\omega\tau} - j\frac{\sigma}{\omega\varepsilon_0} \quad (2)$$

where, ε_s is the static permittivity, $\varepsilon\infty$ is the permittivity at infinite frequency, τ is the relaxation time, and σ is the conductivity of the dielectric. In polyimide, polarization primarily arises from dipolar

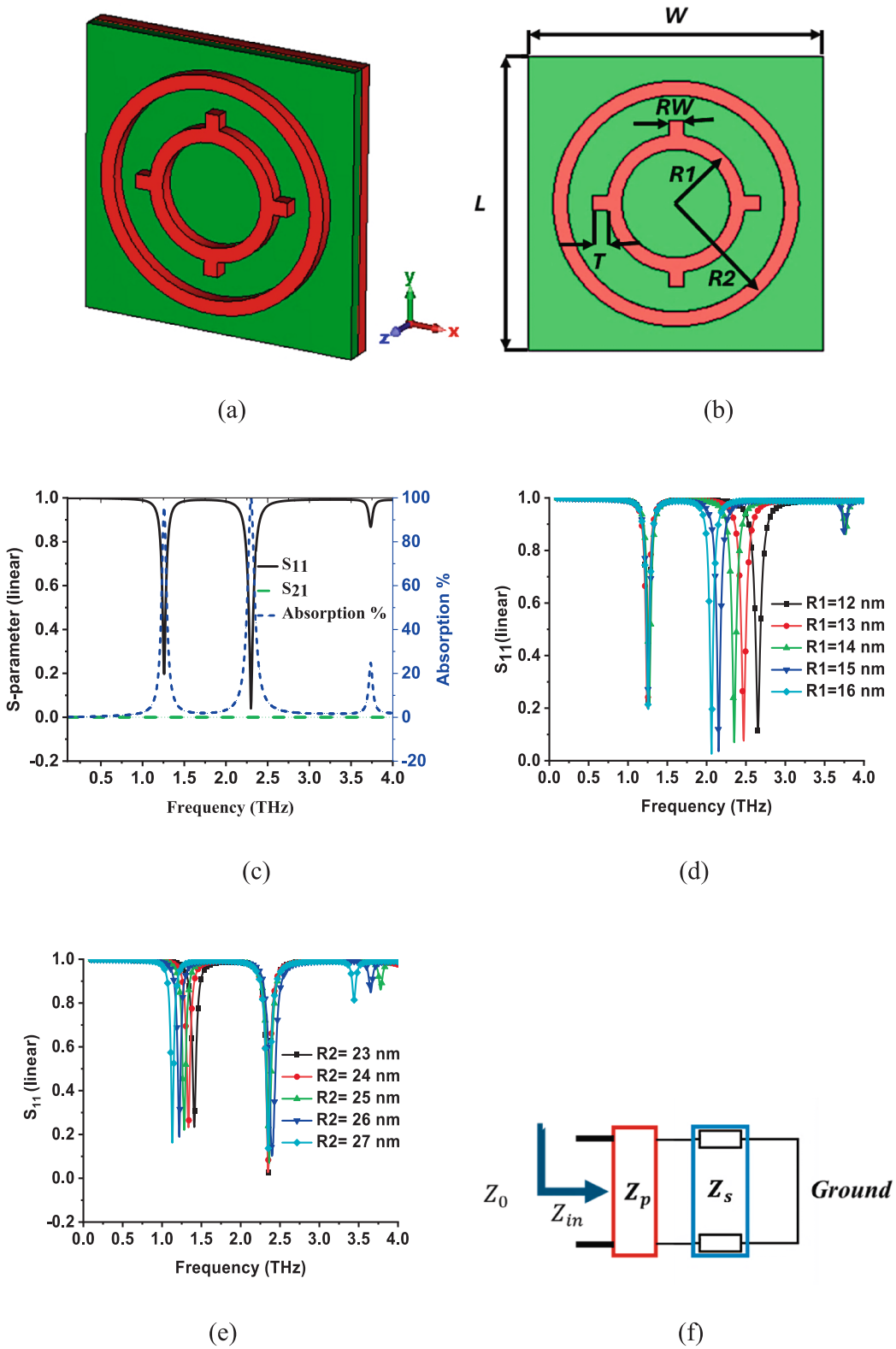

Fig. 1. Proposed Symmetric Dual-Ring Cross Stub (SDR-CS) Absorber (a) perceptive view, (b)front view, (c) S-parameters and absorption %. ($L = 60$ μm, $w = 60$ μm, $R1 = 25$ μm, $R2 = 14$ μm, $RW = 3$ μm, and $T = 3$ μm,), (d) Parametric investigation for inner ring, (e) parametric investigation for outer ring, and (f) Equivalent circuit model of the proposed SDR-CS metamaterial absorber.

orientation and interfacial polarization mechanisms. When an oscillating terahertz (THz) electric field is applied, molecular dipoles attempt to align with the field, but their response is delayed due to the finite relaxation time, resulting in dielectric dispersion and absorption losses. The imaginary part of the permittivity represents this energy loss, which in polyimide is relatively small (loss tangent, tanδ≈0.0027), thereby enabling strong electromagnetic field confinement with minimal dielectric loss. This low-loss dielectric behavior, combined with the

stability of polyimide in the THz regime, makes it highly suitable for metamaterial absorber applications (Jepsen et al., 2011)

Furthermore, the choice of aluminum and polyimide is also motivated by their excellent thermal stability in practical operating conditions. Aluminum maintains high conductivity up to elevated temperatures far beyond standard laboratory environments, while polyimide exhibits a high glass transition and decomposition temperature (>250 °C) with minimal variation in dielectric constant and loss tangent in the 20–80 °C range (Ashby and Jones, 2013). This ensures that under normal ambient conditions, the proposed absorber maintains stable electromagnetic performance without degradation in absorption characteristics, making it reliable for real-world THz sensing and stealth applications. The full-wave electromagnetic simulations were conducted in CST Microwave Studio using the Frequency Domain Solver. To simulate an infinite periodic array of unit cells, unit cell boundary conditions were applied along the x- and y-directions. The structure is excited using Floquet ports on the z-axis, allowing the analysis of the absorber's behavior under TE and TM mode plane wave excitation. The simulated frequency range spans from 0.1 THz to 5 THz, covering the operational bandwidth of interest. The reflection coefficient S_{11} is extracted for normally incident wave excitation, shown in Fig. 1(c). The symmetrical design ensures that results are polarization-independent at normal incidence, as verified through simulations using different polarization angles. Figures (d) and (e) illustrate the parametric analysis of the proposed dual-ring cross-stub absorber with respect to the inner and outer ring radii, respectively. As shown in the geometry, the structure consists of an inner circular resonator (R1) and an outer circular resonator (R2), which together form the dual-band response. The results indicate that the inner ring (R1) predominantly governs the upper resonant band, while the outer ring (R2) primarily contributes to the lower resonant band. Variation of R1 from 12 nm to 16 nm causes a noticeable shift in the upper resonance frequency, confirming its strong influence on the high-frequency mode. Conversely, tuning R2 between 23 nm and 27 nm leads to a significant shift in the lower resonance frequency, highlighting its dominant role in the low-frequency mode. This dual-resonator mechanism provides the flexibility to independently control the two resonance bands, enabling precise tuning for sensing applications in the THz region. The unit cell of the proposed symmetric dual-ring cross-stub (SDR-CS) metamaterial absorber can be modeled as an equivalent inductive-capacitive circuit shown in Fig. 2(f). In this framework, the resonant frequencies of the absorber are determined by the effective inductance and capacitance of the structure, where L_0 corresponds to the length of the T-shaped metal strips combined with the square ring for the lower resonant frequency, or without the square ring for the higher resonant frequency. It is well established that an increase in effective capacitance C results in a narrower full-width at half-maximum (FWHM) and, consequently, a higher quality factor (Q), enhancing the selectivity of the absorber (Wang et al., 2023; Ebrahimi et al., 2020). To further understand the absorption mechanism, the equivalent circuit model of the absorber is illustrated in Fig. 3. Here, *Z*0 represents the free-space wave impedance, *ZA* denotes the overall impedance of the absorber, *ZM* corresponds to the impedance of the metamaterial resonator, and *Z*1 describes the impedance of the substrate layer backed with an aluminum ground plane. The substrate-backed layer can be approximated as a short-circuited transmission line with a length equal to the substrate thickness. Perfect absorption at the dual resonant frequencies is achieved when *ZA* is closely matched to *Z*0, ensuring minimal reflection. This model provides an intuitive understanding of the absorber's dual-band performance and supports further parametric analyses and optimization.

3. Results and performance analysis

3.1. Polarization insensitive

Fig. 2 illustrates the absorption performance of the proposed symmetric dual-ring cross-stub (SDR-CS) metamaterial absorber under varying polarization angles in both the transverse electric (TE) and transverse magnetic (TM) modes. Specifically, Fig. 2(a) presents the absorption spectra for polarization angles ranging from 0° to 90° under TE polarization, while Fig. 2(b) shows the corresponding results for TM polarization. The results clearly indicate that the absorber maintains nearly identical absorption characteristics for all polarization angles. The two resonant peaks, centered around 1.26 THz and 2.29 THz, consistently exhibit near-unity absorption levels exceeding 99 % in both TE and TM modes. This stable performance across the entire polarization range is achieved due to the rotationally symmetric design of the resonating patch, which guarantees a uniform electromagnetic response regardless of the incident electric field orientation. Therefore, the absorber demonstrates polarization-insensitive behavior, which is highly advantageous for practical sensing applications where the polarization state of incident terahertz waves may be arbitrary or uncontrolled.

3.2. Incident angle stability

Fig. 3 illustrates the absorption performance of the proposed SDR-CS metamaterial absorber under varying incident angles for both transverse electric (TE) mode (Figure a) and transverse magnetic (TM) mode (Figure b). The absorption spectra are plotted against frequency in the

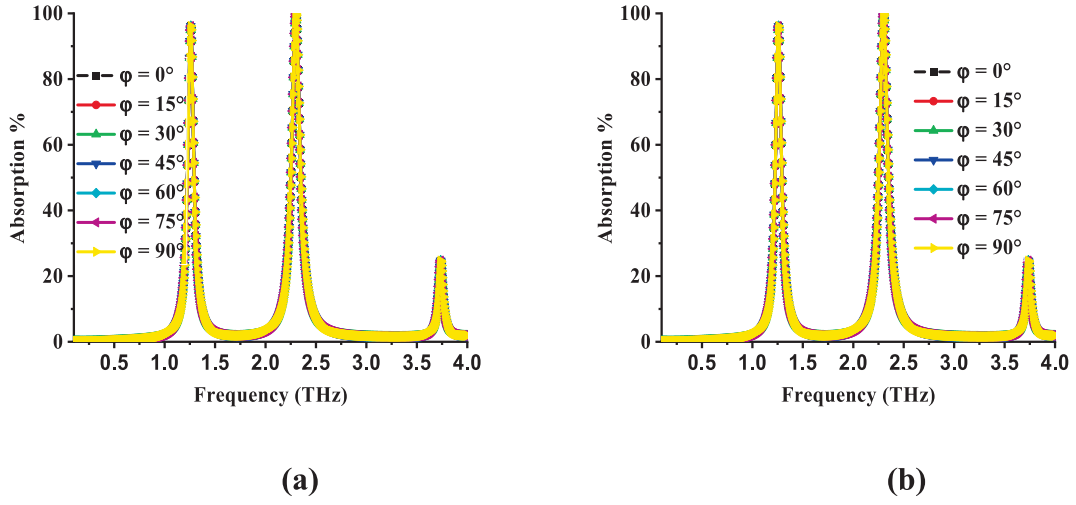

Fig. 2. Absorption of SDR-CS absorber for different polarization angles at (a) TE mode, and (b) TM mode.

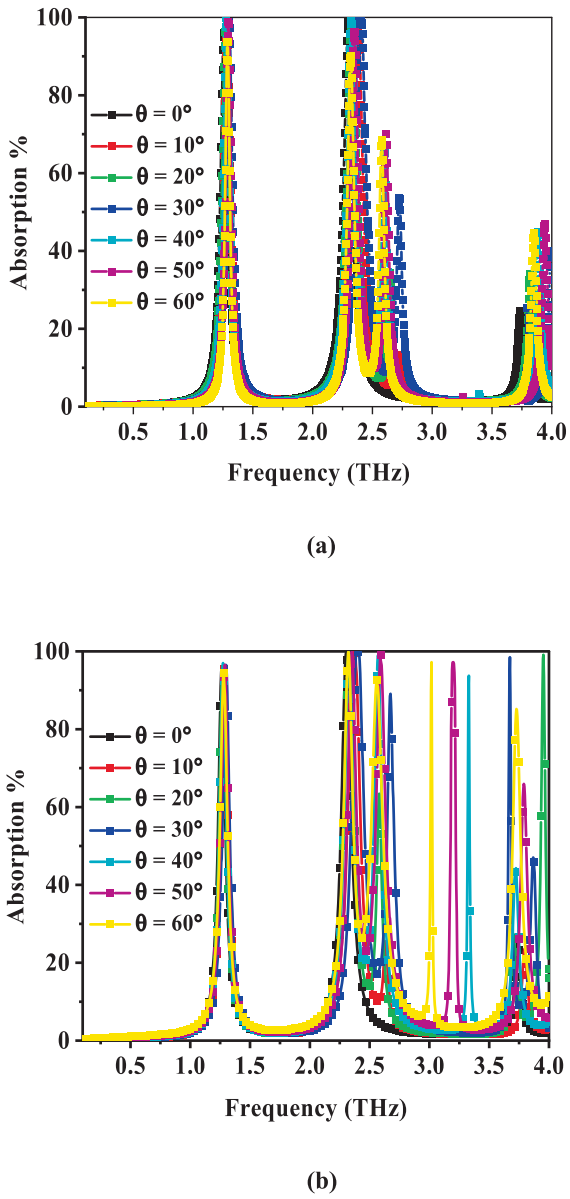

Fig. 3. Absorption of proposed SDR-CS metamaterial absorber at different incident angle. (a) TE mode, and (b) TM mode.

range of 0.1 THz to 4.0 THz for incident angles (θ) ranging from 0° to 60°, in 10° increments. At normal incidence (θ = 0°), the absorber achieves near-unity absorption, with over 99 % absorption occurring at two resonance frequencies: 1.26 THz and 2.29 THz. These strong absorption peaks highlight the resonant behavior of the metamaterial structure, driven by its tailored geometry and electromagnetic response. For the TE mode (Figure a), the absorption remains relatively stable across incident angles, with minimal shift in resonance frequency and only slight degradation in peak absorption at higher angles (θ > 40°). This indicates good angular stability and polarization-insensitive behavior in TE mode. In contrast, the TM mode (Figure b) shows a more pronounced shift in resonance frequencies and a slight reduction in absorption as the incident angle increases. Despite this, high absorption is still maintained over a broad range of angles, confirming the robustness and efficiency of the SDR-CS absorber under different polarization conditions. Overall, the results demonstrate that the proposed absorber not only supports strong dual-band absorption at normal incidence but also maintains good angular tolerance for both TE and TM polarizations.

3.3. Electric and magnetic field distributions at resonance frequencies

Fig. 4 illustrates the simulated electric (E-field) and magnetic (H-field) distributions of the proposed SDR-CS metamaterial absorber at its two peak absorption frequencies, 1.26 THz and 2.29 THz, under both transverse electric (TE) and transverse magnetic (TM) polarizations. The top two rows represent the E-field intensities, and the bottom two rows represent the H-field intensities for the respective polarizations and frequencies. At 1.26 THz, the E-field distributions under both TE and TM incidences exhibit strong localization around the inner and outer ring structures of the resonator. Notably, the electric field is intensely concentrated in the circular gap regions and at the junctions of the cross-stub arms. This field confinement indicates strong capacitive coupling and resonant energy storage. The field symmetry in both TE and TM cases suggests polarization-insensitive behavior at this frequency. The corresponding H-field plots at 1.26 THz reveal a pronounced magnetic field around the central circular region for both TE and TM modes. The TM mode demonstrates slightly more enhanced magnetic activity, indicating strong magnetic dipole excitation. The loop-like magnetic distribution confirms the fundamental resonance behavior essential for efficient absorption. At the higher resonant frequency of 2.29 THz, the E-field patterns shift toward the rectangular cross-stub extensions, especially under TE polarization, where the fields are concentrated along the horizontal arms. This suggests that the outer geometrical features contribute dominantly at this frequency. Under TM polarization, the E-field maintains symmetric excitation along both vertical and horizontal arms, again highlighting polarization insensitivity. The H-field distribution at 2.29 THz for both TE and TM modes forms distinct loops between the cross-stub arms. In particular, the TE mode shows a more concentrated magnetic field along the horizontal arms, whereas the TM mode produces a more circular magnetic confinement pattern. These observations point to the excitation of a higher-order magnetic resonance mode. Overall, the field intensity profiles demonstrate significant electric and magnetic field enhancement in both TE and TM modes at the respective resonance frequencies. This confirms the dual-band nature and polarization-insensitive operation of the proposed SDR-CS absorber. The distinct field localization patterns at 1.26 THz and 2.29 THz validate the excitation of different resonant modes, contributing to strong and stable absorption performance across multiple polarizations.

4. Sensing applications

To evaluate the sensing performance of the proposed symmetric dual-ring cross-stub metamaterial absorber, a dielectric material-under-test (MUT) with varying relative permittivity values is positioned on the absorber, as illustrated in Fig. 5. The primary purpose of varying the permittivity of the MUT is to assess how the electromagnetic properties of the MUT influence the absorption characteristics of the metamaterial absorber (Wang et al., 2023; Banerjee et al., 2025). The MUT serves to perturb the local electromagnetic field distribution of the absorber, thereby altering its effective resonant conditions and shifting its absorption peaks in a predictable manner. A parametric study is conducted for relative permittivity values ranging from 1 to 10. By introducing dielectric materials with different permittivity values onto the absorber, shifts in the absorption peaks are observed, reflecting the sensor's sensitivity to changes in the material's electromagnetic properties. These shifts allow precise tracking of the dielectric properties, enabling the absorber to function as an effective refractive index sensor for applications in material characterization, environmental monitoring, and biosensing (Hakim et al., 2023; Al-Naib, 2018; Saadeldin et al., 2019; Appasani, 2022; Zhang et al., 2022; Rezagholizadeh et al., 2020; Veeraselvam et al., 2021). The corresponding absorption spectra are shown in Fig. 6. As observed, the two primary absorption peaks exhibit a progressive redshift with increasing MUT permittivity/refractive index. Specifically, the lower resonant frequency migrates from 1.2622 THz at $\varepsilon_r = 1$ to 0.9424 THz at $\varepsilon_r = 10$. Simultaneously, the higher resonance

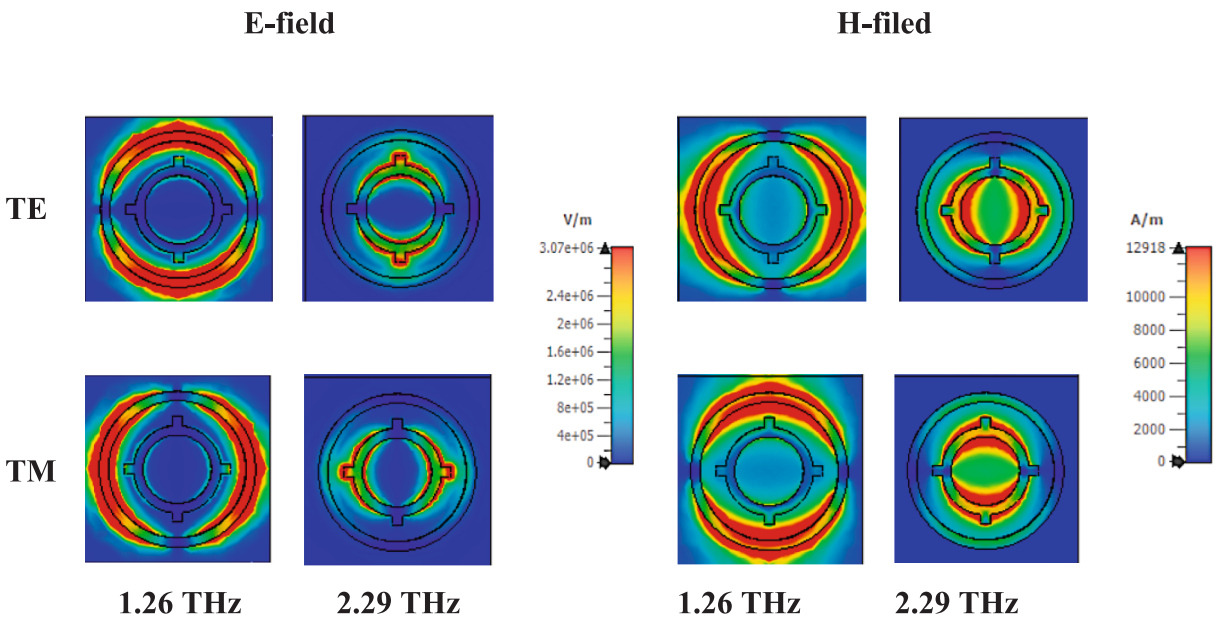

Fig. 4. Proposed SDR-CS metamaterial absorber electric and magnetic field distributions at resonance frequencies.

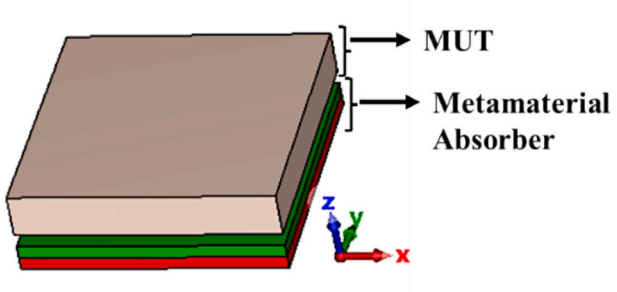

Fig. 5. Proposed sensor setup (MUT thickness 5 mm).

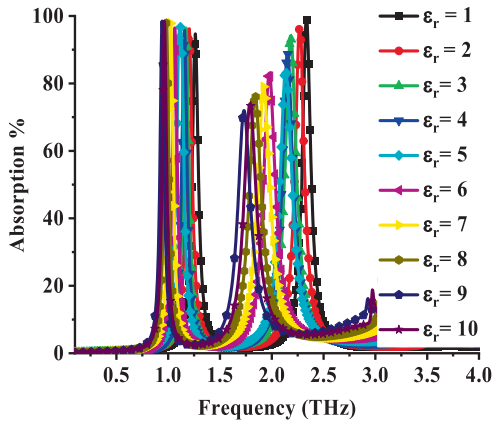

Fig. 6. Absorption plot for different permittivity values of MUT.

shifts from 2.3347 THz to 1.7302 THz over the same range. This consistent downshift in frequency demonstrates the absorber's high sensitivity to the dielectric loading effect introduced by the MUT. Table 2 summarizes these results quantitatively, listing the extracted peak frequencies corresponding to each permittivity/refractive index value. The results clearly indicate a linear and monotonic trend of the frequency shift, which is highly advantageous for reliable permittivity/refractive index characterization. To quantify this relationship, a linear regression is performed between the lower resonant frequency and refrective index. Figs. 7 and 8 (refractive index–based) show the updated regression fits for both sensing bands. Equation (3) is for the shifted frequency calculation of the Lower Sensing Band (Fig. 7):

$$f \text{ lower } (\text{THz}) = 1.43267 - 0.15318n \tag{3}$$

with $R^2 = 0.97773$, adjusted $R^2 = 0.97494$, and Pearson's $r = -0.9888$. The strong linearity and steep slope (–0.15318 THz/unit n) indicate high sensitivity to small changes in refractive index. Equation (4) is for the shifted frequency calculation of the Upper Sensing Band (Fig. 8):

$$f \text{ upper } (\text{THz}) = 2.68231 - 0.28944n \tag{4}$$

with $R^2 = 0.95531$, adjusted $R^2 = 0.94972$, and Pearson's $r = -0.9774$. The greater slope magnitude of –0.28944 THz/unit n highlights the superior responsivity of the upper band. These results confirm the metamaterial absorber's dual-function sensing capability: whether framed in terms of permittivity or refractive index, both resonance bands show high linearity, steep response, and robust performance. This makes the absorber a strong candidate for high-resolution material characterization, environmental monitoring, and biosensing across the THz regime.

The sensitivity of the proposed metamaterial absorber can also be characterized with respect to the refractive index (nnn) of the material under test (MUT), rather than permittivity. This is particularly useful for materials whose dielectric properties are more commonly expressed in terms of nnn, especially in optical and THz domains. Based on the linear regression models obtained for the refractive index-dependent shifts, For the lower resonance band (Fig. 7), the slope of the linear fit is −0.15318 THz per unit refractive index. This corresponds to a sensitivity of $S_1 =$ 153.18 GHz/unit. For the upper resonance band (Fig. 8), the slope of the linear fit is –0.28944 THz per unit refractive index, indicating even higher sensitivity of $S_2 = 289.44$ GHz/unit The negative slope in both cases indicates a redshift in the resonance frequency as the refractive index increases, consistent with the increase in effective optical path length and stored electromagnetic energy due to the MUT. Both sensing bands demonstrate excellent linear correlation coefficients (adjusted R^2 = 0.97494 for the lower band and 0.94972 for the upper band), confirming high accuracy and robustness of the sensor response. These results validate the dual-band metamaterial absorber as a highly sensitive and linear THz refractive index sensor, making it suitable for

Table 2
Comparison with the existing works.

Ref. No	Resonator Design	Materials Used	f (THz)	Size	Range of n	S (GHz/RIU–1)	Q	FOM (RIU–1)
(Al-Naib, 2018)	Symmetric SRR (Fano resonance)	Gold, Polyimide	1.267	120 × 120	1.0–2.0	40	1.5	–
(Zhang et al., 2022)	Metal–Graphene Hybrid	Gold, Graphene, Polyimide	0.1, 1.9	84 × 84	1.4–2.6	285	32	9.02
(Saadeldin et al., 2019)	Complementary Split Ring Resonator (CSRR)	Gold, Silicon	2.249	36 × 36	1.35–1.39	319.6	22.1	2.94
(Rezagholizadeh et al., 2020)	Graphene Disk Resonator	Graphene, SiO_2 substrate	3, 6	65 × 65	1.0–1.8	834	40.1	11.75
(Appasani, 2022)	Hexagonal Ring Resonator	Gold, Polyimide	1.931	160 × 160	1.31–1.39	1045	178.7	–
(Ma et al., 2020)	Centrosymmetric F-shaped Resonator	Gold, Polyimide	5.92	36 × 36	1.1–1.4	1800	49.6	15
(Veeraselvam et al., 2021)	Multiband Ring Resonator	Gold, Polyimide	1.09, 2.8, 4.06	40 × 40	1.0–2.45	514.28	13.89	2.257
(Wang et al., 2023)	Dual-band Square Ring Resonator	Gold, Polyimide	0.715, 1.013	120 × 120	1.0–2.0	152.1, 98.3	–-	–-
(Shruti et al., 2023)	Reconfigurable U-shaped Ring	Polyimide	3.045	100 × 100	1.0–1.03	3.01	86	–-
(Banerjee et al., 2025)	All-Metal Hollow π-shaped	Metal	5.972–7.934	200 × 200	1.0–2.0	5.67–11.03	–-	–-
Proposed work	symmetric dual-ring cross-stub	Al, polyamide	1.26, 2.29	80 × 80	1–3.162	148, 280	32.3, 39.3	3.79, 4.79

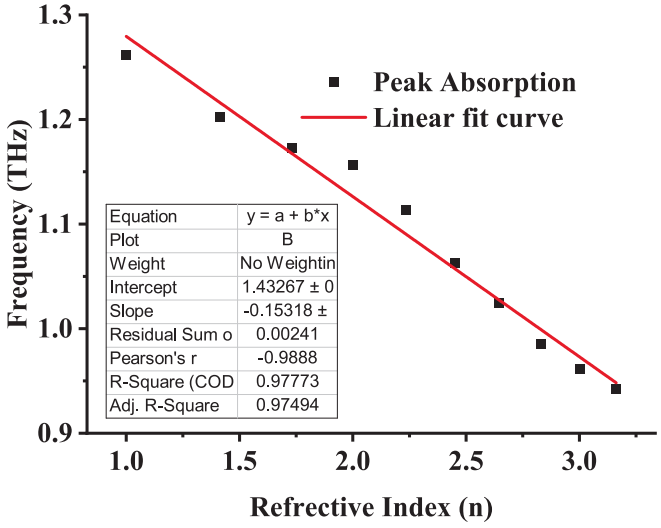

Fig. 7. Fit curve for lower sensing band.

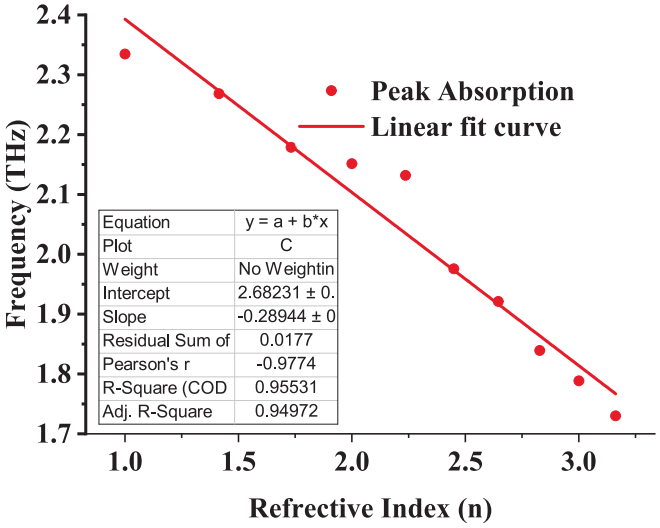

Fig. 8. Fit curve for upper sensing band.

applications in chemical detection, biosensing, and precise material identification. The sensing performance of the proposed symmetric dual-ring cross-stub (SDR-CS) metamaterial absorber has been evaluated in terms of its quality factor (Q-factor) and figure of merit (FOM). The Q-factor, describing the sharpness of the resonance, is calculated as: $Q = f_\circ/\Delta f$ where f_0 is the resonance frequency and Δf is the full-width at half-maximum (FWHM) bandwidth. For the lower resonance at 1.2583 THz with a FWHM of 0.039 THz, the Q-factor is approximately 32.3. Similarly, for the upper resonance at 2.2996 THz with a FWHM of 0.0585 THz, the Q-factor is approximately 39.3. In addition, the figure of merit (FOM) for refractive index sensing, defined as the ratio of sensitivity to FWHM, $FoM = S/\Delta f$ is also evaluated, where S represents the resonance frequency shift per refractive index unit (RIU). For the lower band with a sensitivity of 0.148 THz/RIU, the FOM is approximately 3.79 RIU–1, while the upper band achieves an FOM of 4.79 RIU–1 with a sensitivity of 0.28 THz/RIU. These results demonstrate that the proposed absorber exhibits high frequency selectivity and competitive sensing performance, making it a strong candidate for terahertz sensing, imaging, and stealth applications.

5. Comparison

The proposed SDR-CS (Square Double Ring–Cross Structure) terahertz metamaterial sensor demonstrates superior performance compared to existing designs across multiple key metrics. It offers a significantly broader refractive index sensing range (1–3.162) than most previous works, such as those reported in (Al-Naib, 2018; Saadeldin et al., 2019; Appasani, 2022); enabling wider material detection capabilities. With decent figures of merit (FOM) and strong quality factors (Q) of 32.3 and 39.3 at dual resonance frequencies (1.26 and 2.29 THz), the sensor achieves excellent sensitivity and spectral selectivity, outperforming sensors in (Zhang et al., 2022; Rezagholizadeh et al., 2020; Veeraselvam et al., 2021) Unlike many prior sensors that use gold and polyimide (Al-Naib, 2018; Zhang et al., 2022; Appasani, 2022; Wang et al., 2023) the proposed design utilizes aluminum and polyamide, offering a cost-effective and fabrication-friendly alternative without compromising performance. Its moderate size (80 × 80 μm^2) ensures compactness suitable for integration into lab-on-chip systems, compared to larger designs such as in (Al-Naib, 2018) and (Appasani, 2022; Shruti

et al., 2023; Banerjee et al., 2025). Overall, the proposed sensor surpasses existing works in sensitivity, range, and practicality, making it a strong candidate for high-resolution terahertz sensing applications in biomedical and chemical detection.

6. Conclusion

This paper presented a symmetric dual-ring cross stub (SDR-CS) based dual-band terahertz metamaterial absorber designed for highly sensitive permittivity sensing applications. The proposed absorber achieves near-perfect absorption (~99 %) at two distinct resonance frequencies of 1.26 THz and 2.29 THz, enabled by the engineered coupling of dual hexagonal ring resonators and cross stubs. Its rotational symmetry ensures polarization insensitivity, while stable absorption performance is maintained for incident angles up to 60° in both TE and TM modes, demonstrating excellent angular tolerance. Detailed electromagnetic simulations and field distribution analyses confirmed the dual-band resonance mechanisms responsible for strong electric and magnetic field confinement. Furthermore, the absorber exhibited highly linear and sensitive responses to variations in the permittivity and refractive index of materials placed in proximity, with sensitivity values of 153.18 GHz/RIU and 289.44 GHz/RIU for the lower and upper resonance bands, respectively. Compared to existing THz metamaterial sensors, the proposed SDR-CS design demonstrates clear novelty by offering: (i) a wider sensing range (1–3.162), (ii) dual-band operation with high Q-factors (32.3 and 39.3) and FOM values (3.79 and 4.79), (iii) the use of cost-effective aluminum and polyamide materials instead of conventional gold/polyimide, and (iv) compact geometry suitable for integration into lab-on-chip platforms. These features collectively establish the SDR-CS absorber as a strong candidate for next-generation compact, efficient, and versatile THz sensing platforms with applications in biomedical diagnostics, chemical analysis, and environmental monitoring.

CRediT authorship contribution statement

Ahmed Alqurashi: Writing – original draft, Software, Methodology. **Sayeeda Khanam:** Formal analysis, Data curation, Conceptualization. **Esam Y.O. Zafar:** Visualization, Investigation. **Ahmed J.A. Al-Gburi:** Writing – review & editing, Validation, Project administration.

Declaration of competing interest

The authors declare that they have no known competing financial interests or personal relationships that could have appeared to influence the work reported in this paper.

Acknowledgment

The authors extend their appreciation to Umm Al-Qura University, Saudi Arabia for funding this research work through grant number: 25UQU4340107GSSR01.

Funding Statement

This research work was funded by Umm Al-Qura University, Saudi Arabia under grant number: 25UQU4340107GSSR01.

Data availability

Data will be made available on request.

References

Al-Naib, I., 2018. Thin-film sensing via fano resonance excitation in symmetric terahertz metamaterials. J. Infrared Millimeter Terahertz Waves 39 (1), 1–5.
Appasani, B., 2022. A hybrid terahertz metamaterial sensor using a hexagonal ring resonator with bio-medical applications. Plasmonics 17 (2), 519–524.
Ashby, M.F., Jones, D.R.H., 2013. An introduction to microstructures and processing.
Banerjee, S., Ghosh, I., Santini, C., Mangini, F., Citroni, R., Frezza, F., 2025. All-Metal metamaterial-based sensor with novel geometry and enhanced sensing capability at terahertz frequency. Sensors 25 (2), 507.
Bisht, S.S., Kumar, A., Jhariya, D.K., 2025. A review on electromagnetic metamaterial absorbers and its application. Compact Flexible Microwave Devices 151–195.
Chen, Y.-S., et al., 2023. Terahertz refractive index sensor based on tunable patterned graphene absorber. Diam. Relat. Mater. 131, 109537.
Chen, C., Chai, M., Jin, M., He, T., 2022. Terahertz metamaterial absorbers. Adv. Mater. Technol. 7 (5), 2101171.
Cong, L., Tan, S., Yahiaoui, R., Yan, F., Zhang, W., Singh, R., 2015. Experimental demonstration of ultrasensitive sensing with terahertz metamaterial absorbers: A comparison with the metasurfaces. Appl. Phys. Lett. 106 (3).
Ebrahimi, A., Ako, R.T., Lee, W.S., Bhaskaran, M., Sriram, S., Withayachumnankul, W., 2020. High-$ Q $ terahertz absorber with stable angular response. IEEE Trans. Terahertz Sci. Technol. 10 (2), 204–211.
Hakim, M.L., et al., 2022a. Ultrawideband polarization-independent nanoarchitectonics: a perfect metamaterial absorber for visible and infrared optical window applications. Nanomaterials 12 (16), 2849.
Hakim, M.L., et al., 2022b. Wide-oblique-incident-angle stable polarization-insensitive ultra-wideband metamaterial perfect absorber for visible optical wavelength applications. Materials 15 (6), 2201.
Hakim, M.L., Alam, T., Almutairi, A.F., Mansor, M.F., Islam, M.T., 2021. Polarization insensitivity characterization of dual-band perfect metamaterial absorber for K band sensing applications. Sci. Rep. 11 (1), 17829.
Hakim, M.L., Alam, T., Islam, M.T., Baharuddin, M.H., Alzamil, A., Islam, M.S., 2022. Quad-band polarization-insensitive square split-ring resonator (SSRR) with an inner Jerusalem cross metamaterial absorber for Ku-and K-Band sensing applications. Sensors 22 (12), 4489.
Hakim, M.L., Alam, T., Islam, M.T., Alsaif, H., Soliman, M.S., 2023. Polarization-independent fractal square splits ring resonator (FSSRR) multiband metamaterial absorber/artificial magnetic conductor/sensor for Ku/K/Ka/5G (mm-Wave) band applications. Measurement 210, 112545.
Hu, X., et al., 2016. Metamaterial absorber integrated microfluidic terahertz sensors. Laser Photonics Rev. 10 (6), 962–969.
Jepsen, P.U., Cooke, D.G., Koch, M., 2011. Terahertz spectroscopy and imaging–Modern techniques and applications. Laser Photonics Rev. 5 (1), 124–166.
Landy, N.I., Sajuyigbe, S., Mock, J.J., Smith, D.R., Padilla, W.J., 2008. Perfect metamaterial absorber. Phys. Rev. Lett. 100 (20), 207402.
Linyang, G., Xiaohui, M., Zhaoqing, C., Chunlin, X., Jun, L., Ran, Z., 2021. Tunable a temperature-dependent GST-based metamaterial absorber for switching and sensing applications. J. Mater. Res. Technol. 14, 772–779.
Liu, N., Mesch, M., Weiss, T., Hentschel, M., Giessen, H., 2010. Infrared perfect absorber and its application as plasmonic sensor. Nano Lett. 10 (7), 2342–2348.
Ma, A., et al., 2020. Ultrasensitive THz sensor based on centrosymmetric F-shaped metamaterial resonators. Front. Phys. 8, 584639.
Nie, P., Zhu, D., Cui, Z., Qu, F., Lin, L., Wang, Y., 2020. Sensitive detection of chlorpyrifos pesticide using an all-dielectric broadband terahertz metamaterial absorber. Sens. Actuators B 307, 127642.
Nipun, M.M.K., Islam, M.J., Moniruzzaman, M., 2025. A dual-band perfect terahertz metamaterial absorber for environmental monitoring applications. Phys. Scr. 100 (8), 085506.
Nipun, M.M.K., Islam, M.J., Moniruzzaman, M., 2025. An optimal ultra-thin broadband polarization-independent metamaterial absorber for visible and infrared spectrum applications. Electron. Lett 61 (1), e70314.
Nipun, M.M.K., Islam, M.J., Moniruzzaman, M., 2025. A triple-band metamaterial absorber for gas sensing and refractive index detection through enhanced FOM and Q-factor performance in the THz regime. Results Opt. 21, 100822.
Nipun, M.K., Moniruzzaman, M., Ahmed, F.S., Rana, S.R., Morshed, M.G., 2025. From narrowband to wideband: a review of metamaterial absorber design and development. IUBAT Rev. 8 (1), 145–175.
Pahadsingh, S., Appasani, B., 2024. metamaterial-based terahertz absorbers for refractive index sensing: types, mechanism, and applications. Plasmonics 1–15.
Rezagholizadeh, E., Biabanifard, M., Borzooei, S., 2020. Analytical design of tunable THz refractive index sensor for TE and TM modes using graphene disks. J. Phys. D Appl. Phys. 53 (29), 295107.
Saadeldin, A.S., Hameed, M.F.O., Elkaramany, E.M., Obayya, S.S., 2019. Highly sensitive terahertz metamaterial sensor. IEEE Sens. J. 19 (18), 7993–7999.
Shao, L., et al., 2025. graphene terahertz metamaterials absorber with multiple absorption peaks and adjustable incident polarization angle. Phys. BCondens. Matter, 417427.
Shruti, S.P., Appasani, B., 2024. Metamaterial-based terahertz absorbers for refractive index sensing: types, mechanism, and applications. Plasmonics 1–15.
Shruti, S., Pahadsingh, B., Appasani, A., Srinivasulu, N.B., Thounthong, P., 2023. A reconfigurable terahertz metamaterial absorber for gas sensing applications. Crystals 13 (2), 158.
Veeraselvam, A., Mohammed, G.N.A., Savarimuthu, K., Vijayaraman, P.D., 2021. An ultra-thin multiband refractive index-based carcinoma sensor using THz radiation. IEEE Sens. J. 22 (3), 2045–2052.
Wang, W., et al., 2024. A review of terahertz metamaterial sensors and their applications. Opt. Commun. 556, 130266.
Wang, D., Xu, K.-D., Luo, S., Cui, Y., Zhang, L., Cui, J., 2023. A high Q-factor dual-band terahertz metamaterial absorber and its sensing characteristics. Nanoscale 15 (7), 3398–3407.

Xu, X., Xu, R., Lin, Y.-S., 2022. A voltage-controllable VO_2 based metamaterial perfect absorber for CO_2 gas sensing application. Nanoscale 14 (7), 2722–2728.
Zhang, D., et al., 2022. Dynamically tunable terahertz metamaterial sensor based on metal–graphene hybrid structural unit. AIP Adv. 12 (2).
Zhao, C., Zhao, C.Z., Werner, M., Taylor, S., Chalker, P., 2013. Dielectric relaxation of high-k oxides. Nanoscale Res. Lett. 8 (1), 456.
Zhou, H., et al., 2019. Terahertz biosensing based on bi-layer metamaterial absorbers toward ultra-high sensitivity and simple fabrication. Appl. Phys. Lett. 115 (14).